

# Time resolved synthetic aperture terahertz impulse imaging

K. McClatchey, M. T. Reiten, and R. A. Cheville<sup>a)</sup>

School of Electrical and Computer Engineering, Oklahoma State University, Stillwater, Oklahoma 74078

(Received 11 July 2001; accepted for publication 11 October 2001)

Using a well characterized terahertz (THz) impulse ranging system we demonstrate broad bandwidth imaging at THz frequencies using an inverse synthetic aperture deconvolution technique. The system demonstrates millimeter and submillimeter resolutions along the cross range and range axes, respectively. The range resolution, determined by the THz pulse bandwidth is 0.12 mm, while the cross range resolution is 1.2 mm; both resolutions agree well with theoretical predictions. Through imaging of cylindrical targets we demonstrate quantitative measurement of target position in the image plane within the experimental error of 0.2 mm. Imaging of geometrically scaled complex targets is demonstrated for a 1:2400 scale model ship (1 mm=24 m) corresponding to a full scale frequency bandwidth of 83–625 MHz at a distance of 840 m. © 2001 American Institute of Physics. [DOI: 10.1063/1.1427745]

The ability to optoelectronically generate picosecond electromagnetic pulses with terahertz (THz) bandwidth have permitted realistic and well characterized table-top electromagnetic scattering of geometrically scaled objects at a manageable laboratory scale.<sup>1–3</sup> Applications of such a system include target imaging and analysis, nondestructive evaluation, medical imaging, and remote sensing. The use of THz frequencies for imaging is of great interest due to their ability to penetrate dielectric materials which are opaque or highly scattering to light. Furthermore the  $\omega^2$  absorption coefficient dependence of many materials at THz frequencies permit high contrast in imaging.

In THz impulse ranging, a target is illuminated with optoelectronically generated THz pulses<sup>4</sup> and the scattered field is detected. The generated THz pulses can have bandwidths of over 1 THz, signal to noise ratio as high as  $10^4:1$  in amplitude ( $10^8:1$  in intensity), and intensity polarization extinction ratio of over 1000:1. The optically gated receiver directly measures the electric field phase coherently. The ability to directly measure phase permits determination of the physical shape of the scatterer using some form of image deconvolution.<sup>5</sup> The technique employed here is inverse synthetic aperture imaging.<sup>6,7</sup> This technique is similar to optical holography, however direct phase coherent measurements of electric fields permit image reconstruction without interference with a reference wave in a recording medium. Here we report on imaging of reflective, opaque objects by THz impulse measurements of the scattered electric field. We observe a wide variation between the spatial resolution along the scattered  $\mathbf{k}$  vector (range axis) and orthogonal to it (cross range axis).

The experimental setup for the THz impulse range, schematically represented in Fig. 1(a), is similar to previous THz ranging work.<sup>1–3</sup> THz pulses are generated by illuminating an optoelectronic source chip with ultrashort pulses ( $\sim 80$  fs) from a Ti-sapphire mode-locked laser, collected by a silicon lens, then collimated by an off-axis paraboloidal mirror. The THz beam on the target has an approximately Gaussian profile<sup>8</sup> with a  $1/e$  field half width of 15 mm. The paraboloidal mirror serves to provide a frequency independent spot size at the target.<sup>1</sup> The THz pulses are scattered by the target and a receiver module, located at the variable bistatic angle,  $\beta$ , is used to detect the scattered waveforms. The optoelectronic receiver chip is fiber coupled to the optical gating pulse through a 2 m length of single mode fiber. To compensate for the group velocity dispersion the optical beam is precompensated using a grating pair. The optical pulse measured after the fiber cable has an autocorrelation width of 120

ps. The THz pulses are scattered by the target and a receiver module, located at the variable bistatic angle,  $\beta$ , is used to detect the scattered waveforms. The optoelectronic receiver chip is fiber coupled to the optical gating pulse through a 2 m length of single mode fiber. To compensate for the group velocity dispersion the optical beam is precompensated using a grating pair. The optical pulse measured after the fiber cable has an autocorrelation width of 120

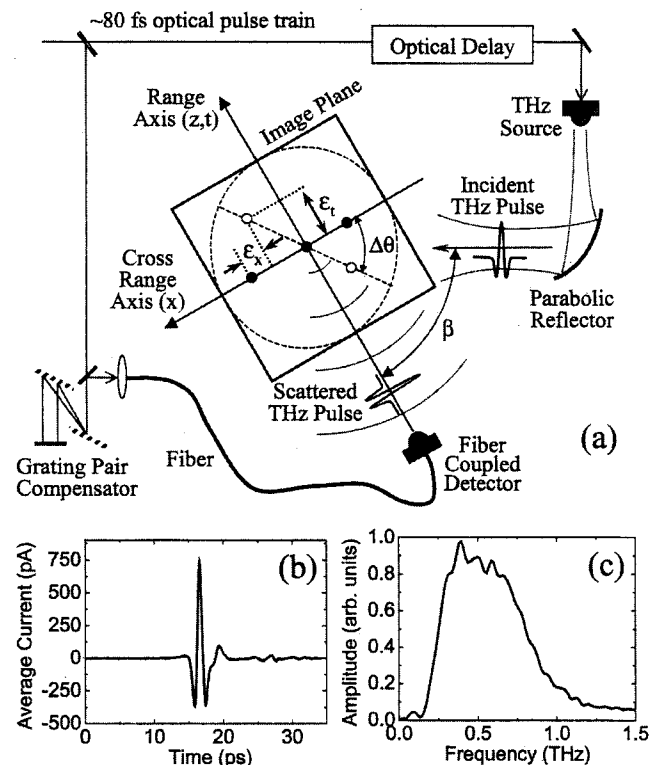


FIG. 1. (a) Schematic diagram of the THz impulse range. The range axis is defined along the line between the stage rotation axis and receiver. The rotation axis-source line is at the bistatic angle,  $\beta$ . Rotation of the stage by  $\Delta\theta$ , shown by the dashed lines, results in movement of the target along the cross range axis by  $\epsilon_x$  and range axis  $\epsilon_r$ , resulting in position errors; (b) THz excitation pulse measured for  $\beta=180^\circ$ ; (c) amplitude spectrum of pulse shown in (b).

<sup>a)</sup>Electronic mail: kridnix@okstate.edu

fs. A wire grid polarizer with power extinction ratio of better than 1000:1 provides polarization sensitivity of the receiver. A low-noise current amplifier in conjunction with a lock-in amplifier measures the average current collected by the receiver dipole, proportional to electric field amplitude.<sup>4</sup> The measured pulse with the receiver located  $\beta=180^\circ$  is shown in Fig. 1(b) and the spectral amplitude in Fig. 1(c).

For synthetic aperture imaging, the receiver module measures the time dependent scattered field at various angles with respect to the target space. On the THz impulse range shown in Fig. 1(a) this can be done either holding the target fixed and moving the receiver, or the receiver can be held fixed as the target is rotated on a center axis. The receiver position, given by the bistatic angle,  $\beta$ , can be varied over the range  $15^\circ$  to  $270^\circ$  with  $0.3^\circ$  resolution. The target rotation can vary from  $0^\circ$  to  $345^\circ$  with a resolution of  $\Delta\theta = 0.001^\circ$ . Here a series of time resolved data scans are acquired as a function of the target position,  $\theta$ . The two-dimensional data array (electric field as a function of time and angle) collected with this impulse range configuration thus permits two-dimensional target spaces in the  $x$ - $z$  plane (parallel to the plane of the page in Fig. 1) to be imaged. Three-dimensional targets which extend in the  $y$  direction have a response determined by the scattering cross section of the target, incident beam profile, and far field pattern of the THz receiver. Path length differences along the  $\hat{y}$  direction cause phase shifts of the detected radiation for out of plane targets, reducing scattered signal. For the 30 mm diameter THz beam size at the target, calculated radius of curvature of the incident THz beam, and 355 mm target to receiver distance the maximum phase shift corresponds to 11.3 radians at 1.0 THz and 2.3 radians at 0.2 THz.

To extract the target image from the temporally resolved data scans taken at angular increments of  $\Delta\theta$ , inverse synthetic aperture imaging treats the target as a superposition of point scatterers. The measured signal at each angular position is a superposition of the field from each point scatterer multiplied by a distance dependent phase shift,  $\Phi$ , determined from the path length from THz source to a particular location on the target to the receiver. To reconstruct the image of the target, the time resolved data are Fourier transformed into the frequency domain and the complex amplitude measured at each value of  $\theta$  is multiplied by the phase shift computed for a particular point,  $x_0$ , on the cross range axis. The net result of this phase shift is to shift the time resolved data along the temporal axis for each angular measurement an amount such that if a scatterer is present at  $x_0$ , all  $\theta$  dependent scans are in phase. In this case a linear superposition of all the scans taken at different  $\theta$  values will sum constructively. If no scatterer is present, the linear superposition will sum destructively. The linear superposition of all scans is made at each value of  $x_0$ , then the data is then inverse transformed into the time domain, yielding a plot of scattering amplitude as a function of  $x_0$  and  $t=z/c$ .

The phase shift term,  $\Phi$ , is determined by the total optical path of the THz pulse from the THz source to target to THz detector as shown in Fig. 1(a). The range (time) axis of the image plane is defined to be along the line from detector to target. The phase shift term is thus a function of frequency,  $\omega$ , the bistatic angle,  $\beta$ , rotation of the image plane,  $\theta$ , and

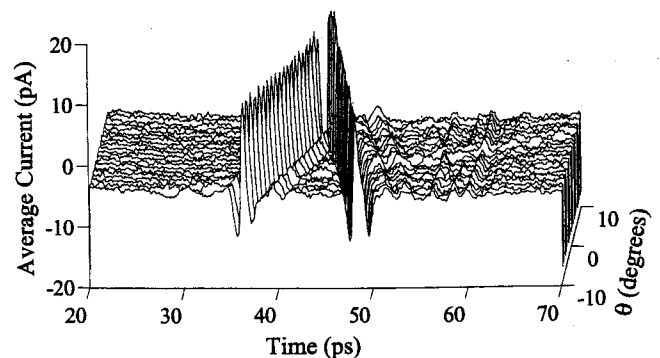


FIG. 2. Waterfall plot of the time resolved scattering signals from two 0.5 mm diameter cylinders measured over a  $20^\circ$  angular range with  $1^\circ$  resolution.

cross range position,  $x_0$ . To simplify the analysis, we assume the target is illuminated by a spherical wave from the source. Given that the incident THz beam is well described by a Gaussian profile,<sup>8</sup> this assumption is valid outside the Rayleigh range of the beam, which for our configuration is valid for frequencies greater 0.3 THz. Detailed methods of calculating the phase shift can be found in several references<sup>6,7</sup> and will be discussed in a subsequent paper.

The image deconvolution algorithm assumes a scatterer remains at a given  $x$  position,  $x_0$ , on the cross range axis and at the origin of the range axis for all scans. As shown by the dashed lines in Fig. 1(a), as the image plane rotates in  $\theta$ , the actual position of the scatterers varies by the amount  $\epsilon_x = x_0(1 - \cos\theta)$  along the cross range axis and  $\epsilon_r = x_0 \sin\theta$  along the range axis. This difference in assumed versus actual positions causes a degradation of the synthetic aperture image. The region of acceptable image degradation is calculated for small  $\theta$  (within paraxial limit) assuming an allowable phase error of  $\pi/2$  and is approximately  $0.25\lambda/[1 - \cos(\theta/2)]$  along the cross range axis and  $\lambda/\theta^2$  along the range axis.<sup>7</sup> This limits the target size to a region of 3.8 by 2.2 mm due to the submillimeter wavelengths comprising the THz pulse. In order to extend this image size the time and angle resolved scattering data matrix is range corrected using a conformal mapping (interpolation) procedure prior to image processing.<sup>6</sup>

Angle resolved scattering measurements were performed for a variety of targets. To calibrate the range we first used two 0.5 mm diameter steel cylinders spaced 5 mm apart as a target. The cylinders were positioned to an accuracy of  $\pm 0.2$  mm. The time resolved data scans taken over a  $\theta$  range of  $20^\circ$  with  $1^\circ$  resolution are shown in Fig. 2 for a bistatic angle of  $\beta=15^\circ$ . The synthetic aperture image obtained from the above data is shown in Fig. 3. The slight skew of the data in the image plane is due to the bistatic angle,  $\beta$ , of  $15^\circ$ . The scatterer positions can be determined by direct measurement from the image, and agree within the experimental error of 0.2 mm to the actual scatterer positions.

As can be seen in Fig. 3, there is a large difference between resolution of the THz impulse range along the range and cross range directions. The resolution along the cross range axis is determined by the angular rotation extent of the data scans given approximately by  $\Delta x = \lambda \times [2 \sin(\theta/2)]^{-1}$  from the condition that the phase shift,  $\Phi$ , varies  $\pi$  radians over the  $\theta$  extent of the aperture.<sup>7</sup> For a  $20^\circ$  range of  $\theta$  the

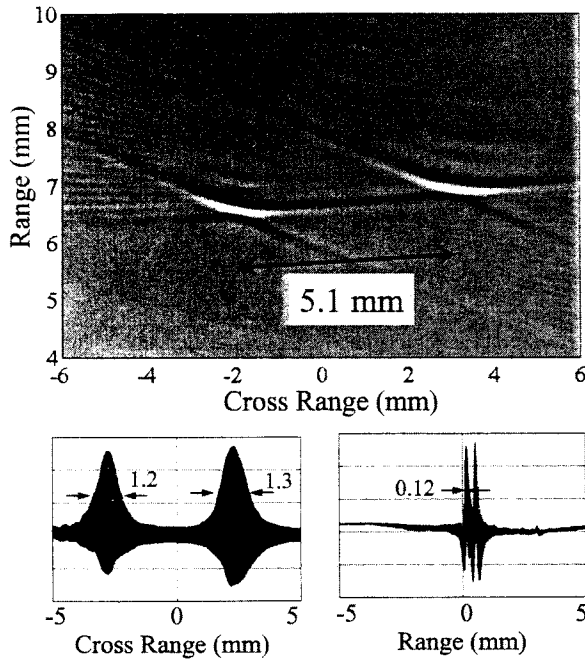


FIG. 3. Deconvolved image obtained from the data in Fig. 2. The figures show the measured image peaks projected onto the cross-range axis (left-hand side) and range axis (right-hand side) show a  $10\times$  difference in resolution.

cross range resolution ranges from 4.3 mm at 0.2 THz to 0.6 mm at 1.5 THz. Along the range direction the resolution is determined by the spatial extent of the THz pulse, determined by the spectral bandwidth. For the pulse shown in Fig. 1(b) with a rise time of  $\Delta t = 0.8$  ps the range resolution is approximately  $\Delta t/2 \times c$  (for small  $\beta$ ) or 0.12 mm, or a factor of ten better than the cross range resolution.

The factor of 10 difference between the range and cross-range resolutions of the THz impulse range can be seen by viewing the measured peaks from the range and cross-range directions in the lower portion of Fig. 3. Applying the Rayleigh criterion to the time resolved data along the range axis, the spatial separation between image peak minimum and maximum is 0.12 mm, in agreement with the predicted value of  $120 \mu\text{m}$  range resolution. The cross-range resolution, measured as the full width at half maximum (FWHM) of the THz pulse, is 1.2 and 1.3 mm for the positive going part of the two scatterers, again in agreement with the predicted values from the measured pulse bandwidth.

To demonstrate the ability of the THz impulse synthetic aperture range to characterize geometrically scaled complex targets, ranging data were acquired on a 1:2400 scale metal "Arleigh Burke" class destroyer. The model has an overall length of 65 mm, extending outside the THz beam. The actual size of this type ship is  $\sim 155$  m. The upper portion of Fig. 4 shows a high contrast photograph of a portion the metal model used, with a scale indicating length. The lower portion of the figure is the image extracted from data taken over a  $20^\circ$  angular range with  $1^\circ$  resolution. The range and cross range axes are shown both in actual model size (mm) and scaled size (m). The data scans used to create the image had a peak signal of 150 pA, with a signal to noise ratio of 75:1. Despite the relatively low number of scans used to create this image, the superstructure and side of the ship are

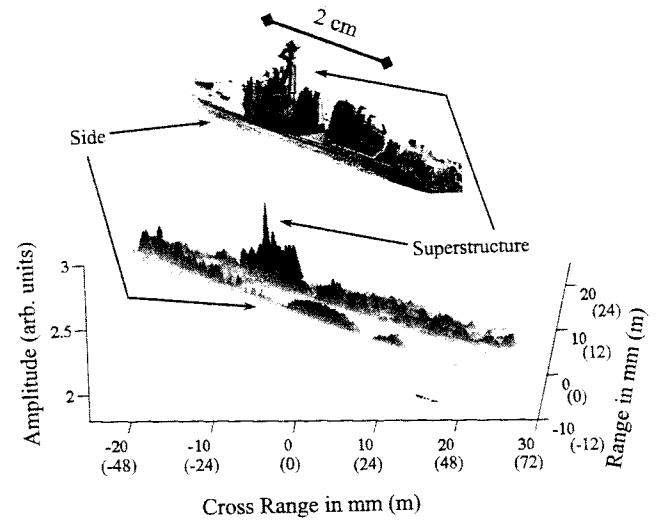


FIG. 4. High contrast photograph of a 1:2400 destroyer model above a THz impulse SAR image taken with  $20^\circ$  angular range and  $1^\circ$  resolution. The sides and superstructure of the model are visible in the image. The axis values in parentheses are the distances in meters which correspond to the scaled image.

clearly resolvable in the image. Note that while the main superstructure with the antenna masts is clearly visible in both the range and cross range directions, the large structure immediately astern, or to the right, is not well imaged. This is due to a slight angle of the flat face of this target feature, which directs a major portion of the scattered THz radiation out of the plane of the measurement. Rotation of the target around two orthogonal axes would be required to fully resolve the target. For the  $2400\times$  scale factor used here, the THz pulse bandwidth, which ranges from 0.2 to 1.5 THz, corresponds to a frequency range of 83–625 MHz with a target to receiver distance of 840 m.

We have demonstrated remote imaging of both simple and complex opaque targets using synthetic aperture tabletop THz impulse ranging. A factor of ten difference between range and cross range resolution is observed, consistent with the THz bandwidth of the excitation pulse. Target features can be quantifiably measured with submillimeter resolution after reconstruction using modified ISAR algorithms.

The authors would like to acknowledge Wendy Seimens for assisting in the construction of this experiment. K.M. would like to acknowledge support of the NSF REU Program. This work was partially supported by the National Science Foundation and Army Research Office.

<sup>1</sup>R. A. Cheville, R. W. McGowan, and D. Grischkowsky, *IEEE Trans. Antennas Propag.* **AP-45**, 1518 (1997).

<sup>2</sup>R. A. Cheville, R. W. McGowan, and D. Grischkowsky, *Phys. Rev. Lett.* **80**, 269 (1998).

<sup>3</sup>R. W. McGowan, R. A. Cheville, and D. Grischkowsky, *Appl. Phys. Lett.* **76**, 670 (2000).

<sup>4</sup>D. Grischkowsky, S. Keiding, M. van Exter, and C. Fattinger, *J. Opt. Soc. Am. B* **7**, 2006 (1990).

<sup>5</sup>A. B. Ruffin, J. Decker, L. Sanchez-Palencia, L. Le Hors, J. F. Whitaker, T. B. Norris, and J. V. Rudd, *Opt. Lett.* **26**, 681 (2001).

<sup>6</sup>M. Soumekh, *Synthetic Aperture Radar Signal Processing* (Wiley, New York, 1999).

<sup>7</sup>D. L. Mensa, *High Resolution Radar Imaging* (Artech House, Dedham, MA, 1981).

<sup>8</sup>P. Uhd Jepsen and S. R. Keiding, *Opt. Lett.* **20**, 807 (1995).